

Record-high Anomalous Ettingshausen effect in a micron-sized magnetic Weyl semimetal on-chip cooler

Mohammadali Razeghi¹, Jean Spièce¹, Valentin Fonck¹,
 Yao Zhang^{3,4}, Michael Rohde¹, Rikkie Joris², Philip S. Dobson⁵,
 Jonathan M. R. Weaver⁵, Lino da Costa Pereira²,
 Simon Granville^{3,4}, Pascal Gehring^{1*}

^{1*}IMCN/NAPS, Université Catholique de Louvain (UCLouvain), Street,
 Louvain-la-Neuve, 1348, Belgium.

²QSP, KUL, Street, Leuven, 1587, Belgium.

³Robinson Research Institute, Victoria University of Wellington,
 Wellington, PO Box 600, New Zealand.

⁴MacDiarmid for Advanced Materials and Nanotechnology, Wellington,
 PO Box 600, New Zealand.

⁵James Watt School of Engineering, University of Glasgow, Glasgow,
 G12 8LT, United Kingdom.

*Corresponding author(s). E-mail(s): pascal.gehring@uclouvain.be;

Abstract

Solid-state cooling devices offer compact, quiet, reliable and environmentally friendly solutions that currently rely primarily on the thermoelectric (TE) effect. Despite more than two centuries of research, classical thermoelectric coolers suffer from low efficiency which hampers wider application. In this study, the less researched Anomalous Ettingshausen effect (AEE), a transverse thermoelectric phenomenon, is presented as a new approach for on-chip cooling. This effect can be boosted in materials with non-trivial band topologies as demonstrated in the Heusler alloy Co_2MnGa . Enabled by the high quality of our material, in situ scanning thermal microscopy experiments reveal a record-breaking anomalous Ettingshausen coefficient of -2.1 mV in μm -sized on-chip cooling devices at room temperature. A significant 44% of the effect is contributed by the intrinsic

topological properties, in particular the Berry curvature of Co_2MnGa , emphasising the unique potential of magnetic Weyl semimetals for high-performance spot cooling in nanostructures.

Keywords: Anomalous Ettingshausen effect, Magnetic Weyl semimetals, topology, on-chip spot-cooling

Main

The constraints that typically limit the efficiency of conventional thermoelectric materials where heat and charge flow in parallel do not apply to the Ettingshausen effect (EE, see Fig. 1b), a *transverse* thermoelectric phenomenon similar to the Hall effect, where heat and charge currents are orthogonal: When a charge current density \mathbf{J}_c flows through a material exposed to a magnetic field \mathbf{B} , a heat current $\mathbf{J}_{q,EE}$ is generated perpendicularly to both. Thanks to their orthogonality, heat and charge flow

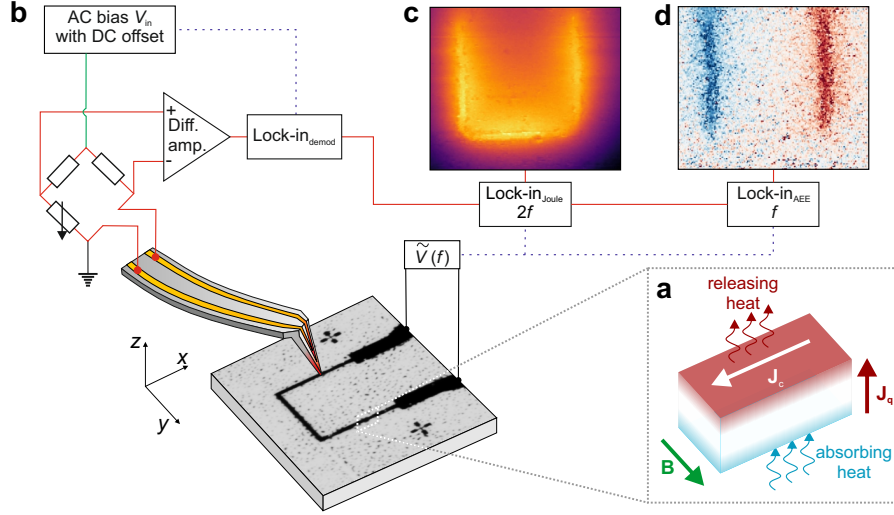


Fig. 1 Schematic of the Scanning Thermal Microscopy experiments used to quantify Ettingshausen cooling. **a**, The charge current density \mathbf{J}_c that flows through an Ettingshausen cooler which is exposed to a magnetic field \mathbf{B} induces a transverse heat flux \mathbf{J}_q which decreases/increases the bottom/top surface temperature. **b**, An AC current J_c is injected into the U-shape Co_2MnGa device (optical micrograph shown) using an AC voltage bias \tilde{V} at frequency f_{exc} (black lines). The SThM tip is biased with a small AC and DC offset (V_{in} , green line) using a Wheatstone bridge. A first lock-in demodulates the signal with respect to the tip excitation. Subsequently, a second lock-in demodulates the second ($2 \times f_{exc}$) and first harmonic (f_{exc}) corresponding to the Joule (**c**) and AEE (**d**) response, respectively. These signals are further converted into temperature variation maps via tip calibration (see methods).

are decoupled, which eliminates Joule heating's parasitic contributions, significantly

boosting conversion efficiency. Consequently, Etingshausen coolers hold the record for the lowest temperature achieved by room temperature thermoelectric cooling [1]. However, the Etingshausen effect typically requires a substantial external magnetic field, often several Tesla, to operate. Recent research has shown that this hurdle can be overcome by leveraging materials with nontrivial band topologies. Akin to the anomalous Hall effect, the thermoelectric counterparts, the anomalous Nernst/Etingshausen effects, depend on the magnetization of the compound and on the anomalous velocity of electrons linked to the band structure’s Berry curvature which can be significant in magnetic materials. Remarkably, a class of quantum materials known as magnetic Weyl semimetals boasts exceptionally large [2] (or even ‘giant’ [3]) anomalous Nernst coefficients due to their topologically non-trivial band structure. This discovery could unlock the high-performance spot cooling potential, as the Nernst and Etingshausen coefficients are closely linked through the Bridgman relation [4]. Nonetheless, precise measurement of cooling effects in nanostructures remains challenging due to limitations in instrumentation or material quality [5], and experimental evidence for such significant Etingshausen cooling efficiency awaits confirmation. Here, we find a record-high anomalous Etingshausen coefficient for on-chip coolers with a μm footprint made of the Heusler alloy Co_2MnGa . To this end, we performed frequency- and magnetic-field-dependent local thermometry and local thermal transport experiments by means of Scanning Thermal Microscopy (SThM). Our findings reveal the important contribution of topology on the transverse thermoelectric effect in our samples and demonstrate that microscale anomalous Etingshausen devices are strong candidates for on-chip cooling applications.

High-quality single-crystalline, epitaxial Co_2MnGa thin films with a thickness of 50 nm were deposited on single-crystalline MgO (001) substrates by DC magnetron sputtering [6]. The Co_2MnGa films are capped by a thin Ta layer to prevent oxidation (see Methods for details). Since the heat current $\mathbf{J}_{\text{q,AEE}}$ generated by the Anomalous Etingshausen Effect (AEE) depends on the direction of the charge current density \mathbf{J}_c and the magnetization \mathbf{M} (unit vector \mathbf{m}) by [7, 8]

$$\mathbf{J}_{\text{q,AEE}} = \Pi_{\text{AEE}} \cdot (\mathbf{J}_c \times \mathbf{m}), \quad (1)$$

where the proportionality constant Π_{AEE} is the Anomalous Etingshausen coefficient, we patterned the Co_2MnGa thin films into microscale U-shaped devices (see Methods). This allows parallel and perpendicular \mathbf{m} and \mathbf{J}_c to be realised in a single device, leading to areas without ($\mathbf{J}_c \times \mathbf{m} = 0$), and with positive ($\mathbf{J}_c \times \mathbf{m} > 0$) or negative ($\mathbf{J}_c \times \mathbf{m} < 0$) Etingshausen response, respectively. This geometry further allows differentiation between the Etingshausen effect and other thermoelectric effects like the magneto-Peltier effect [9, 10] (see Supplementary Fig. S1).

To measure the local temperature distribution on Co_2MnGa on-chip coolers with nanometer spatial and mK temperature resolution, we employed an AC-SThM method [11–13] (see Fig. 1a). To this end, the Co_2MnGa U-shaped device is biased by a sinusoidal alternating current (AC) with frequency f and amplitude J_c . Joule heating and Etingshausen cooling/heating can then be obtained by demodulating the thermometer signal of the SThM probe at $2f$ and f , respectively.

Such Joule and AEE temperature maps recorded at a charge current $I_c = 0.952$ mA, $f = 17$ Hz, and in-plane magnetic field of 80 mT are shown in Fig. 1c,d. While Joule heating raises the temperature of the three sides of the U-shaped device equally, the Ettingshausen effect increases (decreases) the temperature in areas where the magnetic field is perpendicular to the current. For areas where the magnetic field is parallel to the charge current, no temperature change is observed, in accordance with Eq. 1.

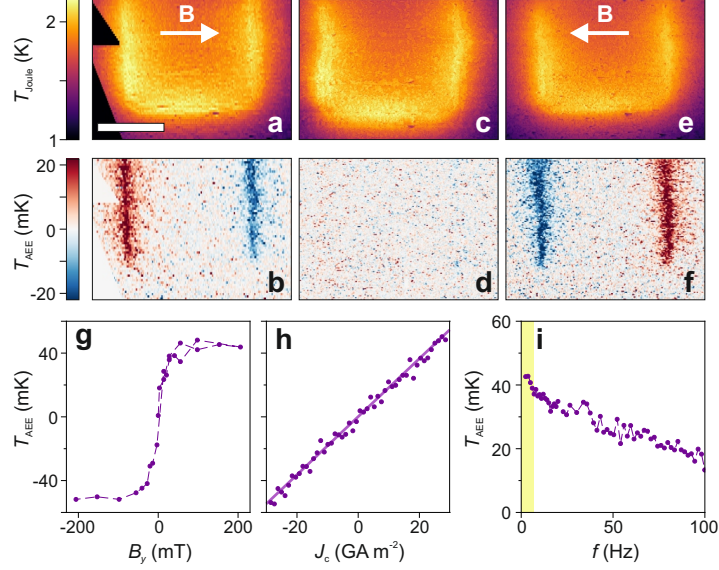


Fig. 2 Anomalous Ettingshausen effect and Joule heating in Co_2MnGa . **a,c,e**, Maps of T_{Joule} and **b,d,f**, T_{AEE} for the U-shaped 50-nm-thick Co_2MnGa film, measured at a frequency of $f=17$ Hz, current density $J_c = 19 \text{ GA m}^{-2}$ (current $I_c = 0.95$ mA) and under a magnetic field B_y of 80 mT (**a,b**), 0 (**c,d**), and -80 mT (**e,f**). **g**, T_{AEE} as a function of magnetic field B_y measured at $J_c = 28.5 \text{ GA m}^{-2}$ and $f = 17$ Hz. **h**, T_{AEE} as a function of charge current density J_c measured at $B_y = 80$ mT and $f = 17$ Hz. Solid line: linear fit to the data. **i**, T_{AEE} as a function of frequency f measured at $J_c = 19 \text{ GA m}^{-2}$ and $B_y = 80$ mT. Scale bar: $10 \mu\text{m}$.

In Fig. 2, we further investigate the magnetic-field dependence of the AEE effect. Figs. 2a, c, e and b, d, f show the Joule and AEE response, respectively, at -80 mT, 0 mT, and 80 mT. We observe AEE maps of similar spatial distribution and amplitude but with opposite sign for -80 mT and 80 mT as expected from Eq. 1. For $\mathbf{B} = 0$ no AEE signal is observed within our experimental resolution limit. The Joule heating maps (Figs. 2a,c,e) are not affected by the magnetic field. To further investigate the influence of frequency, current density, and magnetic field, we placed the SThM probe at a constant location on the right leg of the U-shaped device. The force between the probe and the sample is kept constant using the AFM feedback loop. Fig. 2h illustrates the linear correlation between the T_{AEE} and the applied current density J_c ,

as expected from Eq. 1, with $dT_{\text{AEE}}/dJ_c = 1.8 \times 10^{-12} \text{ m}^2\text{KA}^{-1}$, while a quadratic response is observed in Joule heating (see Supplementary Fig. S2). Fig. 2g shows the magnetic field dependence of the T_{AEE} . We observe a steep increase of the signal at low fields followed by saturation at a field of $B \approx 50 \text{ mT}$, which qualitatively follows the magnetization of our films measured by SQUID (see Supplementary Fig. S3c). Such saturation is the hallmark of an anomalous Ettingshausen effect, and the anomalous Ettingshausen coefficient can be extracted from this saturation region. Lastly, we observe that T_{AEE} decreases with increasing AC frequency of J_c (Fig. 2i). This reflects the thermal response time of the system (the U-shaped device and substrate), which is on the order of tens of milliseconds. Conversely, at low frequencies, the signal maximizes and approaches the steady-state value, which is used to quantify Π_{AEE} .

It is worth mentioning that the spatial temperature distribution in the Joule and AEE maps differs noticeably. As shown in the Supplementary Fig. S3, while Joule heating decays over several μm around the U pattern, AEE heating/cooling is localized around the device. This directly links to the different origins of the produced heat: While the Joule heating is produced uniformly and isotropically throughout the whole film, the AEE heat current is directional and flows alike from heat source to a heat sink located at the top/bottom sides of the device [14]. This confined temperature distribution created by the AEE allows for precise local temperature control that cannot be achieved using conventional methods that have high thermal diffusion.

Using Eq. 1, it is possible to derive an expression for the AEE coefficient Π_{AEE} given by experimentally accessible parameters. Considering T_{AEE} in steady state regime, Π_{AEE} can be expressed as [8, 9, 15]:

$$\Pi_{\text{AEE}} = \frac{\kappa \cdot 2T_{\text{AEE}}}{J_c \cdot L}, \quad (2)$$

where κ is the thermal conductivity and L is the thickness of the film. A factor of 2 is introduced to account for the temperature difference between the top and bottom of the sample. We measured κ by SThM (see Supplementary Information Section 6) and find a value of $22 \pm 4 \text{ W K}^{-1} \text{ m}^{-1}$. Using this value we obtain $\Pi_{\text{AEE}} = -2.1 \pm 0.4 \text{ mV}$. This agrees well with the value $\approx -2.3 \text{ mV}$ estimated using the Bridgman relation $\Pi_{\text{AEE}} = S_{\text{ANE}} * T$ and the experimental anomalous Nernst coefficient of our films [16]. In Fig. 3a we compare Π_{AEE} of Co_2MnGa normalized by the magnetization M to values reported in literature (filled shapes). Since only a few studies have experimentally quantified Π_{AEE} , we added estimated values for the anomalous Ettingshausen coefficient (hollow shapes) using the experimental Nernst effect coefficient S_{ANE} and applying the Bridgman relation [17, 18]. Furthermore, consistent with previous reports on anomalous transport coefficients [9, 15, 19], Fig. 3a shows that Π_{AEE} of Co_2MnGa does not scale with magnetization values (trivial scaling indicated by the gray-shaded area). This suggests the involvement of intrinsic material properties, such as a large Berry curvature resulting from the non-trivial band topology.

In the following, we will discuss the origin of the large AEE coefficient measured in Co_2MnGa . The AEE and its Onsager counterpart, the ANE, consist of both intrinsic

(Π_1 and S_1) and extrinsic (Π_2 and S_2) contributions [7–9, 20]:

$$\Pi_{\text{AEE}} = \Pi_1 + \Pi_2 = (S_1 + S_2)T = (\rho_{xx} * \alpha_{xy} + \rho_{xy} * \alpha_{xx})T. \quad (3)$$

Here, ρ_{ij} and α_{ij} are components of resistivity and thermoelectric tensors, respectively. The intrinsic term is a result of the Berry phase which generates an anomalous velocity perpendicular to the applied electric field across occupied states near the Fermi level. The extrinsic term arises from the scattering mechanism induced by effective spin-orbit coupling (SOC) in magnetic materials [21, 22].

To estimate such contributions, we performed magnetoresistance and Hall measurements on our Co_2MnGa films (see Supplementary Fig. S3a and b). Using the experimental values of S_{xx} , Π_{AEE} , ρ_{xx} and ρ_{xy} , we calculate a large transverse thermoelectric coefficient $\alpha_{xy} = -2.14 \text{ A (K m)}^{-1}$. This value can be used to estimate Π_1 and Π_2 (see Supporting Information), which we compare to values reported in the literature in Fig. 3b. Notably, Co_2MnGa features the record for the highest Π_{AEE} at room temperature. Furthermore, we find that there is a large contribution of 44% from the Berry curvature Π_1 to the overall anomalous Ettingshausen effect, underlining the importance of the intrinsic topological nature of Co_2MnGa to explain the enormous Π_{AEE} observed in our experiments.

Conclusion

In summary, we report an unprecedented anomalous Ettingshausen effect in spot coolers fabricated from Co_2MnGa thin films with lateral dimensions of $1 \mu\text{m}$. By combining caloric scanning thermal microscopy measurements and electrical magnetotransport experiments, we uncovered a substantial intrinsic anomalous Ettingshausen component due to the large Berry curvature near the Fermi energy of Co_2MnGa . This intrinsic contribution, coupled with the extrinsic counterpart, synergistically enhances the overall cooling efficiency. These results highlight the profound impact of non-trivial band topology on transverse thermoelectric effects and signal transformative potential for a new generation of high-efficiency on-chip coolers. Such advances are poised to address critical needs in thermal management, sensing, healthcare and quantum computing.

Methods

Material synthesis and device preparation

Co_2MnGa film growth

Epitaxial deposition of 50nm Co_2MnGa thin films was carried out using a Kurt J Lesker CMS-18 magnetron sputtering system with a base pressure below 3×10^{-8} Torr on $\text{MgO}(001)$ substrates. Prior to thin film fabrication, substrates were cleaned with Ar plasma and were subsequently annealed at 400°C for 30 minutes in the vacuum chamber. The deposition of Co_2MnGa thin films was performed by DC magnetron sputtering from a stoichiometric polycrystalline target at 100 W under 6 mTorr of Ar,

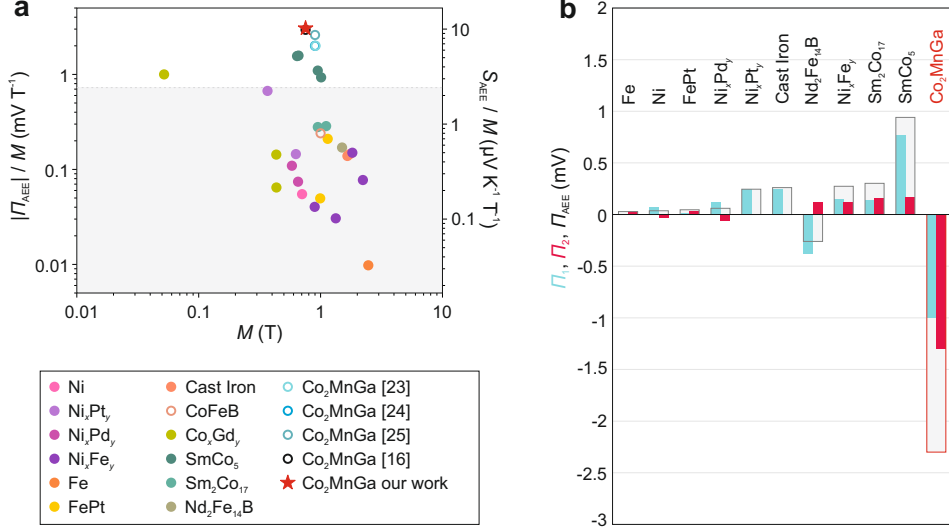


Fig. 3 Comparison of the Ettingshausen coefficient of Co_2MnGa with literature. **a**, Ettingshausen coefficient normalized by magnetization as a function of magnetization. Filled circles: experimental Ettingshausen data; Empty circles: estimations using experimental Nernst data and the Bridgeman relation: 0.5 mm-thick Fe, Ni, $\text{Ni}_{95}\text{Pt}_5$, $\text{Ni}_{75}\text{Pt}_{25}$, $\text{Ni}_{70}\text{Pd}_{30}$, $\text{Ni}_{95}\text{Fe}_5$, $\text{Ni}_{75}\text{Fe}_{25}$, $\text{Ni}_{50}\text{Fe}_{50}$, $\text{Ni}_{25}\text{Fe}_{75}$ and $\text{Fe}_{50}\text{Pt}_{50}$ (ref. [9]), 10 nm-thick FePt (ref. [17]), 1 mm-thick ductile and grey cast iron (ref. [8]), 30 nm-thick $\text{Co}_{86}\text{Gd}_{14}$, $\text{Co}_{78}\text{Gd}_{22}$ and $\text{Co}_{58}\text{Gd}_{42}$ (ref. [19]), 1.5 mm-thick SmCo_5 , $\text{Sm}_2\text{Co}_{17}$ -type magnet and $\text{Nd}_2\text{Fe}_{17}\text{B}$ (ref. [7]), 10 nm-thick CoFeB (ref. [2]), 1.3 mm-thick Co_2MnGa (ref. [23]), 0.5 mm-thick Co_2MnGa (ref. [24]), Single crystal Co_2MnGa (ref. [25]), 50 nm-thick Co_2MnGa (ref. [16]). **b**, Total Ettingshausen coefficient Π_{AEE} (grey bars) and its two contributions Π_1 (blue bars) and Π_2 (red bars). 10 nm-thick Fe, Ni, $\text{Fe}_{50}\text{Pt}_{50}$, $\text{Ni}_{70}\text{Pd}_{30}$, $\text{Ni}_{75}\text{Pt}_{25}$ and $\text{Ni}_{50}\text{Fe}_{50}$ [9], 1 mm-thick cast iron [8], 1.5 mm-thick $\text{Nd}_2\text{Fe}_{17}\text{B}$, SmCo_5 and $\text{Sm}_2\text{Co}_{17}$ [7].

with a growth rate of $0.8\text{\AA}\cdot\text{s}^{-1}$ at 400°C . During the deposition, the sample holder was rotated, and post-annealing was conducted in situ at 400°C for 20 minutes. Following the cooling down to ambient temperature, a 2 nm Ta protective layer was deposited on the top.

Sample Preparation

Hall bars ($l = 2000\ \mu\text{m}$, $w = 150\ \mu\text{m}$) for transport measurements were patterned using photolithography, followed by Ar ion milling. For thermometry measurements, the Co_2MnGa is patterned into U-shaped devices using standard electron beam lithography followed by ion milling. The legs have a length of $20\ \mu\text{m}$, and a channel width of $1\ \mu\text{m}$.

Scanning Thermal Microscopy

Scanning Thermal Microscopy (SThM) was used for both, temperature mapping and thermal conductivity measurements. Measurements were conducted with a Bruker Dimension Icon Atomic Force Microscope (AFM) under ambient conditions using

VITA-DM-GLA-1 probes featuring a palladium heater on a silicon nitride cantilever/tip, with a typical tip radius ranging from 25 to 60 nm. We performed a calibration of the tip radius using a method described elsewhere [26, 27] and obtained 51 nm. The heater, integrated into a modified Wheatstone bridge, was driven by a combined 91 kHz AC and DC bias, as detailed elsewhere [13, 28]. Detection of the signal was achieved through an SR-830 lock-in amplifier, and the amplitude output was directed to the AFM controller.

Temperature measurements

For magnetic field-dependent AC-thermometry measurements, the sample is biased at a frequency of $f = 17$ Hz unless otherwise specified. The SThM tip is driven with $V_{pp} = 4$ V and $V_{DC} = 2$ V at a high frequency of $f = 91$ kHz, resulting in a temperature increase of the tip by $\Delta T_{tip} \approx 7.5$ K. The direct current (DC) signal is recorded using an SRS830 lock-in at the same frequency as the tip excitation. T_{AEE} and T_{Joule} are determined by demodulating the signal using a Zurich Instruments MFLI lock-in amplifier at the 1st and 2nd harmonics while the SThM tip scans over the surface or is held at a constant position. The magnetic field is applied by an home-built electromagnet.

Data availability

The data supporting the findings of this study are available in the Article and its Supplementary Information files. Data sets can be found at <https://doi.org/xxxx>.

References

- [1] Harman, T., Honig, J., Fischler, S., Paladino, A., Button, M.J.: Oriented single-crystal bismuth Nernst-Ettingshausen refrigerators. *Applied Physics Letters* **4**(4), 77–79 (1964)
- [2] Reichlova, H., Schlitz, R., Beckert, S., Swekis, P., Markou, A., Chen, Y.-C., Kriegner, D., Fabretti, S., Hyeon Park, G., Niemann, A., *et al.*: Large anomalous Nernst effect in thin films of the Weyl semimetal Co_2MnGa . *Applied Physics Letters* **113**(21), 212405 (2018)
- [3] Yang, H., You, W., Wang, J., Huang, J., Xi, C., Xu, X., Cao, C., Tian, M., Xu, Z.-A., Dai, J., Li, Y.: Giant anomalous Nernst effect in the magnetic Weyl semimetal $\text{Co}_3\text{Sn}_2\text{S}_2$. *Phys. Rev. Mater.* **4**, 024202 (2020)
- [4] Bridgman, P.: The connections between the four transverse galvanomagnetic and thermomagnetic phenomena. *Physical Review* **24**(6), 644 (1924)
- [5] Mizuno, H., Modak, R., Hirai, T., Takahagi, A., Sakuraba, Y., Iguchi, R., Uchida, K.-i.: Deposition temperature dependence of thermo-spin and magneto-thermoelectric conversion in Co_2MnGa films on $\text{Y}_3\text{Fe}_5\text{O}_{12}$ and $\text{Gd}_3\text{Ga}_5\text{O}_{12}$. *Applied Physics Letters* **120**(20), 202401 (2022)

- [6] Zhang, Y., Yin, Y., Dubuis, G., Butler, T., Medhekar, N.V., Granville, S.: Berry curvature origin of the thickness-dependent anomalous Hall effect in a ferromagnetic Weyl semimetal. *npj Quantum Materials* **6**(1), 17 (2021)
- [7] Miura, A., Sepehri-Amin, H., Masuda, K., Tsuchiura, H., Miura, Y., Iguchi, R., Sakuraba, Y., Shiomi, J., Hono, K., Uchida, K.-i.: Observation of anomalous Ettingshausen effect and large transverse thermoelectric conductivity in permanent magnets. *Applied Physics Letters* **115**(22), 222403 (2019)
- [8] Nagasawa, R., Oyanagi, K., Hirai, T., Modak, R., Kobayashi, S., Uchida, K.-i.: Anomalous Ettingshausen effect in iron-carbon alloys. *Applied Physics Letters* **121**(6), 062401 (2022)
- [9] Miura, A., Iguchi, R., Seki, T., Takanashi, K., Uchida, K.-i.: Spin-mediated charge-to-heat current conversion phenomena in ferromagnetic binary alloys. *Physical Review Materials* **4**(3), 034409 (2020)
- [10] Uchida, K.-i., Daimon, S., Iguchi, R., Saitoh, E.: Observation of anisotropic magneto-Peltier effect in nickel. *Nature* **558**(7708), 95–99 (2018)
- [11] Menges, F., Mensch, P., Schmid, H., Riel, H., Stemmer, A., Gotsmann, B.: Temperature mapping of operating nanoscale devices by scanning probe thermometry. *Nature Communications* **7**(1), 10874 (2016)
- [12] Harzheim, A., Spiece, J., Evangeli, C., McCann, E., Falko, V., Sheng, Y., Warner, J.H., Briggs, G.A.D., Mol, J.A., Gehring, P., *et al.*: Geometrically enhanced thermoelectric effects in graphene nanoconstrictions. *Nano Letters* **18**(12), 7719–7725 (2018)
- [13] Spiece, J., Evangeli, C., Lulla, K., Robson, A., Robinson, B., Kolosov, O.: Improving accuracy of nanothermal measurements via spatially distributed scanning thermal microscope probes. *Journal of Applied Physics* **124**(1), 015101 (2018)
- [14] Das, R., Iguchi, R., Uchida, K.-i.: Systematic investigation of anisotropic magneto-peltier effect and anomalous ettingshausen effect in Ni thin films. *Physical Review Applied* **11**(3), 034022 (2019)
- [15] Miura, A., Masuda, K., Hirai, T., Iguchi, R., Seki, T., Miura, Y., Tsuchiura, H., Takanashi, K., Uchida, K.-i.: High-temperature dependence of anomalous Ettingshausen effect in SmCo₅-type permanent magnets. *Applied Physics Letters* **117**(8), 082408 (2020)
- [16] Hu, J., Zhang, Y., Huo, X., Li, N., Liu, S., Yu, D., Ansermet, J.-P., Granville, S., Yu, H.: Large Anomalous Nernst Angle in Co₂MnGa Thin Film. *IEEE Magnetics Letters* **13**, 1–5 (2022)
- [17] Seki, T., Iguchi, R., Takanashi, K., Uchida, K.: Relationship between anomalous

- Ettingshausen effect and anomalous Nernst effect in an FePt thin film. *Journal of Physics D: Applied Physics* **51**(25), 254001 (2018)
- [18] Xu, L., Li, X., Lu, X., Collignon, C., Fu, H., Koo, J., Fauqué, B., Yan, B., Zhu, Z., Behnia, K.: Finite-temperature violation of the anomalous transverse Wiedemann-Franz law. *Science Advances* **6**(17), 3522 (2020)
- [19] Seki, T., Miura, A., Uchida, K.-i., Kubota, T., Takanashi, K.: Anomalous Ettingshausen effect in ferrimagnetic Co-Gd. *Applied Physics Express* **12**(2), 023006 (2019)
- [20] Sumida, K., Sakuraba, Y., Masuda, K., Kono, T., Kakoki, M., Goto, K., Zhou, W., Miyamoto, K., Miura, Y., Okuda, T., *et al.*: Spin-polarized Weyl cones and giant anomalous Nernst effect in ferromagnetic Heusler films. *Communications Materials* **1**(1), 89 (2020)
- [21] Nagaosa, N., Sinova, J., Onoda, S., MacDonald, A.H., Ong, N.P.: Anomalous hall effect. *Reviews of Modern Physics* **82**(2), 1539 (2010)
- [22] Miyasato, T., Abe, N., Fujii, T., Asamitsu, A., Onoda, S., Onose, Y., Nagaosa, N., Tokura, Y.: Crossover behavior of the anomalous Hall effect and anomalous Nernst effect in itinerant ferromagnets. *Physical Review Letters* **99**(8), 086602 (2007)
- [23] Sakai, A., Mizuta, Y.P., Nugroho, A.A., Sihombing, R., Koretsune, T., Suzuki, M.-T., Takemori, N., Ishii, R., Nishio-Hamane, D., Arita, R., *et al.*: Giant anomalous Nernst effect and quantum-critical scaling in a ferromagnetic semimetal. *Nature Physics* **14**(11), 1119–1124 (2018)
- [24] Guin, S.N., Manna, K., Noky, J., Watzman, S.J., Fu, C., Kumar, N., Schnelle, W., Shekhar, C., Sun, Y., Gooth, J., *et al.*: Anomalous Nernst effect beyond the magnetization scaling relation in the ferromagnetic Heusler compound Co₂MnGa. *npg Asia Materials* **11**(1), 16 (2019)
- [25] Xu, L., Li, X., Ding, L., Chen, T., Sakai, A., Fauqué, B., Nakatsuji, S., Zhu, Z., Behnia, K.: Anomalous transverse response of Co₂MnGa and universality of the room-temperature $\alpha_{ij}^A/\sigma_{ij}^A$ ratio across topological magnets. *Phys. Rev. B* **101**, 180404 (2020)
- [26] Spièce, J., Evangeli, C., Robson, A.J., El Sachat, A., Haenel, L., Alonso, M.I., Garriga, M., Robinson, B.J., Oehme, M., Schulze, J., *et al.*: Quantifying thermal transport in buried semiconductor nanostructures via cross-sectional scanning thermal microscopy. *Nanoscale* **13**(24), 10829–10836 (2021)
- [27] Gonzalez-Munoz, S., Agarwal, K., Castanon, E.G., Kudrynskiy, Z.R., Kovalyuk, Z.D., Spièce, J., Kazakova, O., Patanè, A., Kolosov, O.V.: Direct measurements of anisotropic thermal transport in γ -inse nanolayers via cross-sectional scanning

thermal microscopy. *Advanced Materials Interfaces*, 2300081 (2023)

- [28] Spièce, J.: Quantitative Mapping of Nanothermal Transport Via Scanning Thermal Microscopy. Springer Theses, pp. 1–153. Springer, Nature Switzerland AG (2019). <https://doi.org/10.1007/978-3-030-30813-1>

Supplementary information

Supplementary Figs. 1–6, sections 1–6.

Acknowledgments

P.G., J.S. and V.F. acknowledge financial support from the F.R.S.-FNRS of Belgium (FNRS-CQ-1.C044.21-SMARD, FNRS-CDR-J.0068.21-SMARD, FNRS-MIS-F.4523.22-TopoBrain, FNRS-PDR-T.0128.24-ART-MULTI, FNRS-CR-1.B.463.22-MouleFrits, FNRS-FRIA-1.E092.23-TOTEM). P.G. acknowledges financial support from the EU (ERC-StG-10104144-MOUNTAIN), from the Federation Wallonie-Bruxelles through the ARC Grant No. 21/26-116, and from the FWO and FRS-FNRS under the Excellence of Science (EOS) programme (40007563-CONNECT).

Author information

Contributions

P.G. conceived and supervised the study. Y.Z. and S.G. grew the Co_2MnGa thin films and performed the magnetotransport measurements. R.J. and L.dC.P. performed the SQUID experiments. V.F. and Mi.R. fabricated the U-shaped devices. P.S.D. and J.M.R.W. fabricated the SThM probes. Mo.R., V.F. and J.S. performed the SThM experiments and evaluated the data. Mo.R., J.S. and P.G. wrote the manuscript with input from all co-authors. All authors have given approval to the final version of the manuscript.

Declarations

Conflict of interest

The authors declare no competing interests.